

Linear magnetohydrodynamic response of the magnetopause to magnetosheath fluctuations

J. De Keyser

Belgian Institute for Space Aeronomy, Brussels

Abstract. We study the response of the magnetopause to incident magnetosheath ULF fluctuations by combining the linear magnetohydrodynamics (MHD) approach with harmonic analysis. We consider plane wave fronts arriving at the magnetopause with various tangential wavelengths. The fluctuations in the magnetosheath are pulse trains or waves with a broadband ULF spectrum. We obtain the magnetopause response to these fluctuations based on the computation of the transmission, reflection, and absorption characteristics of monochromatic linear MHD waves at different frequencies in a given equilibrium magnetopause configuration. Particular attention is given to MHD wave mode conversion as an ingredient for explaining the enhanced electromagnetic fluctuation level near the magnetopause.

1. Introduction

The magnetospheric boundary layer separates the shocked solar wind in the magnetosheath from the magnetospheric plasma. This boundary layer usually consists of two parts. The outer part is the magnetopause current layer, which carries the diamagnetic current associated with the transition between the magnetosheath and the magnetospheric magnetic fields. The inner part is the low-/high-latitude boundary layer, generally located on closed magnetic field lines and containing magnetosheath plasma that somehow managed to cross the magnetopause. The overall structure of the magnetospheric boundary can be described by equilibrium models that assume the magnetopause to be locally in a tangential or rotational discontinuity state [e.g., *Sonnerup and Cahill*, 1968; *Lee and Kan*, 1979; *Paschmann et al.*, 1979]. The boundary, however, is strongly affected by transient phenomena. These are particularly important for mass and energy transport across the magnetopause. Such phenomena include flux transfer events, impulsive penetration of plasma, percolation, and diffusion.

In this paper we do not focus on large-scale transient mechanisms that affect the structure of the magnetopause but on the ever-present small-scale ultralow frequency (ULF) fluctuations [*LaBelle and Treumann*, 1988]. These ULF waves are known to exist in the broadband fluctuation spectrum of the solar wind, but they might also be generated in the Earth's vicinity, for instance as turbulence immediately upstream of the quasi-parallel bow shock [*Engebretson et al.*, 1991]. These ULF waves are convected downstream across the bow shock and through the magnetosheath. Different hydromagnetic ULF wave modes have been identi-

fied in the magnetosheath [*Anderson et al.*, 1982; *Song et al.*, 1994; *Lacombe et al.*, 1995]. The ULF fluctuation level generally peaks at the magnetopause and is suppressed in the magnetosphere [*Perraut et al.*, 1979; *Anderson et al.*, 1982; *Rezeau et al.*, 1989; *Engebretson et al.*, 1991; *Rezeau et al.*, 1993; *Song et al.*, 1993]. *Belmont et al.* [1995] were the first to suggest that the peak fluctuation level at the magnetopause not necessarily meant that these fluctuations were generated there by some instability but that this peak could also be due to resonant amplification of the incident magnetosheath fluctuations. Resonant mode conversion of MHD waves, which leads to localized resonant amplification of the wave amplitude, is a well-studied process in different contexts [e.g., *Southwood*, 1974; *Poedts et al.*, 1989; *Zhu and Kivelson*, 1989; *Hollweg*, 1997, and references therein]. Mode conversion occurs at plasma inhomogeneities such as the magnetopause, where the Alfvén and sound speeds change, so that the Alfvén or slow-mode frequencies can match the incident wave frequency at some points. The resonant excitation of tangential Alfvén and slow-mode waves by the incident wave enhances the fluctuation level there.

In the cold plasma case only Alfvén resonances are possible; they are due to the changing Alfvén velocity across the magnetopause [*Belmont et al.*, 1995]. *De Keyser et al.* [1999] discuss the warm plasma case, with changes in plasma parameters and in magnetic field intensity and orientation across the magnetopause, showing the simultaneous presence of multiple resonant layers corresponding to both Alfvén and slow-mode resonances. The present paper further extends this work by considering magnetosheath wave packets or waves with a broadband spectrum, rather than the monochromatic waves used before. This improves the realism of earlier simulations of the magnetosheath wave mode conversion scenario. To this end, we combine the order analysis (linearization, with its implicit limitation to small perturbation amplitude) with harmonic analysis (to reproduce various waveforms and incident wave spectra). The pres-

Copyright 2000 by the American Geophysical Union.

Paper number 2000JA900083.
0148-0227/00/2000JA900083\$09.00

ence of a broadband spectrum leads to resonant absorption of wave energy not in one or a few isolated resonant layers, but the absorption is distributed more evenly throughout the magnetopause.

The merit of this paper lies in the study and interpretation of the effect of broadband ULF fluctuations on the magnetopause. This is of direct relevance for the interpretation of the magnetopause response to the observed magnetosheath wave spectra. We focus here on two types of magnetosheath waves identified by *Anderson et al.* [1982]: (1) We examine the dynamic consequences of intermittent, “spiky” perturbations on the magnetopause. To this end, we consider a periodic density pulse train with a period that is much larger than the pulse duration, in order to avoid interference effects between incident pulses and their reflections. (2) We also study the effects on the magnetopause of ULF continua with substantial power in a broad low-frequency band, like those identified observationally [*Rezeau et al.*, 1989; *Song et al.*, 1994; *Lacombe et al.*, 1995].

2. Geometry and Plasma Properties

We consider the same subsolar magnetopause configuration as *De Keyser et al.* [1999]. The equilibrium is of the tangential discontinuity type without plasma flow, that is, the normal magnetic field $B_x^{(0)} \equiv 0$, and the equilibrium velocity $v^{(0)} \equiv 0$ (x is the coordinate along the Earth–Sun line). The magnetospheric field $B_{\text{msph}}^* = B^{(0)}(-\infty)$ and the magnetospheric and magnetosheath mass densities and (ion + electron) temperatures ρ_{msph}^* , ρ_{msh}^* , T_{msph}^* , T_{msh}^* are given. The (ion + electron) mass is denoted by m . We then adopt the following equilibrium profiles:

$$\begin{aligned}\rho_{\text{msph}}^{(0)}(x) &= \rho_{\text{msph}}^* \mathcal{G}(x/D), \\ \rho_{\text{msh}}^{(0)}(x) &= \rho_{\text{msh}}^* \mathcal{G}(-x/D), \\ \rho^{(0)}(x) &= \rho_{\text{msph}}^{(0)}(x) + \rho_{\text{msh}}^{(0)}(x), \\ T^{(0)}(x) &= [T_{\text{msph}}^* \rho_{\text{msph}}^{(0)}(x) + T_{\text{msh}}^* \rho_{\text{msh}}^{(0)}(x)] / \rho^{(0)}(x), \\ p_{\text{th}}^{(0)}(x) &= k_B \rho^{(0)}(x) T^{(0)}(x) / m,\end{aligned}$$

where $\mathcal{G}(x/D) = \frac{1}{2} \text{erfc}(x/D)$ allows a smooth transition with half width D (erfc denotes the complementary error function). These profiles specify a magnetopause with half thickness D , centered at $x = 0$. In the present paper we will not consider the effects of magnetic field rotation across the magnetopause; the magnetic field remains unidirectional. We adopt the values $\rho_{\text{msph}}^*/m = 1 \text{ cm}^{-3}$, $\rho_{\text{msh}}^*/m = 20 \text{ cm}^{-3}$, $T_{\text{msph}}^* = 20 \times 10^6 \text{ K}$, $T_{\text{msh}}^* = 4 \times 10^6 \text{ K}$, $B_{\text{msph}} = 65 \text{ nT}$, and a magnetopause half thickness $D = 300 \text{ km}$ [*Berchem and Russell*, 1982]. The magnetic field profile is determined from pressure balance, with $B_{\text{msh}} = 46 \text{ nT}$. This equilibrium configuration is shown in Figure 1. It is characterized by Alfvén speeds $v_{A,\text{msh}} = 225 \text{ km s}^{-1} < v_{A,\text{msph}} = 1420 \text{ km s}^{-1}$ and sound speeds $c_{s,\text{msh}} = 235 \text{ km s}^{-1} < c_{s,\text{msph}} = 525 \text{ km s}^{-1}$.

The proton gyrofrequency is 700 mHz in the magnetosheath and 1000 mHz in the magnetosphere, setting an up-

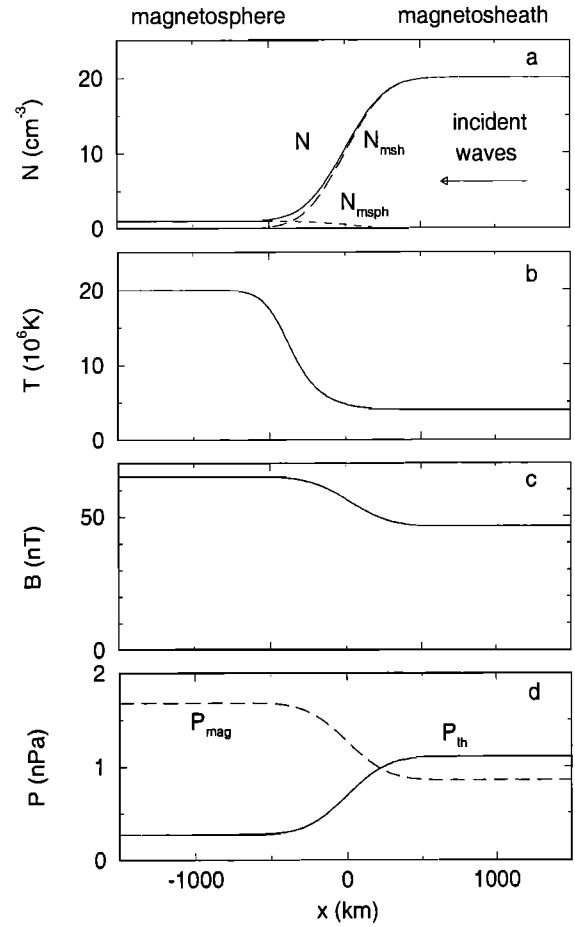


Figure 1. Equilibrium low-shear subsolar magnetopause configuration used in this paper. The characteristic half width of the transition is 300 km: (a) number density, (b) temperature, (c) magnetic field, and (d) thermal and magnetic pressure satisfying pressure balance.

per limit to the frequencies we can safely consider within the MHD approximation. The Alfvén and slow-mode travel times from the subsolar point to the cusp are of the order of hundreds of seconds; the behavior of resonant waves with longer periods (lower frequencies) is affected by the cusp response. We therefore consider frequencies f in the range 5 – 500 mHz (periods 2 – 200 s). For such frequencies we find typical Alfvén wavelengths $\lambda_A = v_A/f = 1500 - 150,000 \text{ km}$ that are much larger than the ion gyroradii $\rho_{\text{msh}} = 58 \text{ km}$ and $\rho_{\text{msph}} = 92 \text{ km}$. The one-dimensional approximation becomes invalid for the largest of these wavelengths as they are of the order of the radius of curvature of the magnetopause. The magnetosheath flow also can no longer be ignored far from the subsolar point. The magnetopause layer was chosen to be sufficiently wide (several ion gyroradii) so that the MHD approximation does apply.

3. Linearization and Harmonic Analysis

We linearize the ideal MHD equations around the equilibrium configuration by writing every quantity (depending on

position \mathbf{r} and time t) as a sum of its equilibrium value and higher order contributions: $q(\mathbf{r}, t) = q^{(0)}(x) + q^{(1)}(\mathbf{r}, t) + \dots$. The linearization procedure (see the Appendix) assumes that every perturbed quantity is smaller than its equilibrium value: $q^{(1)} \ll q^{(0)}$. Such small-amplitude perturbations do not essentially alter the state of the plasma through which they propagate. Therefore the unperturbed plasma properties (and their gradients) completely determine the propagation characteristics of the waves; no wave-wave interactions are taken into account. The response of the system to a superposition of several small-amplitude waves then simply is the superposition of the responses of the system to each individual wave. We exploit this property here to use harmonic analysis in order to compute the system response to small-amplitude wave packets or broadband waves. We consider periodic perturbations $q^{(1)}$ that are composed of waves with frequencies $\omega_{\pm n} = \pm n\omega_{\text{base}} = \pm 2\pi n f_{\text{base}}$, where $n = 1, 2, \dots, n_{\text{max}}$, and with wave vectors $\mathbf{k} = k_x(x)\mathbf{1}_x + \mathbf{k}_t$, where the tangential wave vector $\mathbf{k}_t = [0, k_y, k_z]$ is the same for all frequency components. Such broadband plane wave perturbations are of the form

$$q^{(1)}(\mathbf{r}, t) = \sum_{n=1}^{n_{\text{max}}} \hat{q}_n(x) e^{i(\mathbf{k}_t \mathbf{r} - \omega_n t)} + \hat{q}_{-n}(x) e^{i(\mathbf{k}_t \mathbf{r} + \omega_n t)},$$

that is, the set of \hat{q}_n constitute the discrete Fourier transform of the first-order perturbation. For each frequency ω_n the perturbation $\hat{q}_n(x)$ can be computed from the linearized MHD equations, which can be expressed in terms of the normal displacement $\hat{\xi}_x$ and the total pressure perturbation $\hat{\tau}$ as

$$\begin{aligned} \frac{d}{dx} \hat{\tau} &= C_1(x, \mathbf{k}_t, |\omega_n|) \hat{\xi}_x, \\ \frac{d}{dx} \hat{\xi}_x &= C_2(x, \mathbf{k}_t, |\omega_n|) \hat{\tau}. \end{aligned}$$

Expressions for C_1 and C_2 are given in the Appendix. The perturbation wavelength can be smaller, of the same order, or larger than the equilibrium gradient length scales that appear in the expressions for C_1 and C_2 through the local Alfvén and sound speeds. Note, however, that the wavelength range is limited by the assumptions inherent in the planar MHD problem setup, as discussed in the previous section. In uniform regions, the propagation equations become the simple wave equation

$$\left(\frac{d^2}{dx^2} + K_x^2 \right) \hat{\xi}_x = 0,$$

with $K_x^2 = -C_1 C_2$. As \mathbf{k}_t is real for plane waves, K_x^2 is real as well. If $K_x^2 > 0$ the solution is a superposition of a left- and a right-going sinusoidal wave, with $k_x = \pm K_x$ (propagating waves). If $K_x^2 < 0$, the solution is a superposition of an exponentially growing and decaying mode, with $k_x = \pm i \sqrt{-K_x^2}$ (nonpropagating waves). When C_2 becomes unbounded at some point in the domain (C_1 is always bounded), K_x^2 is unbounded there (when $C_1 \neq 0$) and the wavelength in the normal direction tends to zero, corresponding to resonant absorption. The resonance conditions reflect the coupling between the magnetosonic waves propa-

gating in the x direction and the tangential Alfvén and slow-mode waves at the singular points:

$$\begin{aligned} |k_{\parallel}| &= k_A = \frac{|\omega_n|}{v_A}, \\ |k_{\parallel}| &= k_S = \frac{|\omega_n|}{v_A} \sqrt{v_A^2 + c_s^2}, \end{aligned}$$

k_A and k_S are the local Alfvén and slow-mode wave vectors [Belmont *et al.*, 1995; De Keyser *et al.*, 1999]. Each spectral component is characterized by its proper resonance conditions, and its proper transmission, reflection, and absorption coefficients.

Following Belmont *et al.* [1995], we consider surface wave vectors $\mathbf{k}_t + \epsilon_t i$ that have a small imaginary part ($\epsilon_t/k_t \ll 1$). The wave fronts then are slightly modulated in the tangential direction with a length scale $\sim \epsilon_t^{-1} \gg \lambda_t$, rather than being exactly planar. Introducing this imaginary part avoids the unboundedness of C_2 at the points of resonance. In general, one then has $\text{Im } K_x^2 \neq 0$, implying that the amplitude of a wave propagating in a uniform medium no longer remains constant and that the time averaged energy flux $\langle \phi_x \rangle$ associated with that wave changes with x at a rate proportional to ϵ_t , which must therefore be chosen small enough. The magnitude of the jump in the energy flux at the resonant points is then independent of the precise value of ϵ_t (see the Appendix); the sign of the jump, however, depends on the direction of ϵ_t with respect to the magnetic field and the flow velocity.

4. Boundary Conditions

For the computation of each spectral component we impose boundary conditions on the magnetospheric side: We require that only a left-going wave is present there, implying that $\hat{\tau}(x_{\text{msph}}) = \pm \hat{\xi}_x(x_{\text{msph}}) \sqrt{C_1(x_{\text{msph}})/C_2(x_{\text{msph}})}$, where the sign is chosen so as to select the left-going wave [De Keyser *et al.*, 1999]. As the linear wave solutions for each frequency are determined up to an arbitrary scaling factor, we choose $\hat{\xi}_x(x_{\text{msph}}) = 1$. We solve the differential equations for $\hat{\xi}_x$ and $\hat{\tau}$ using an adaptive second-order implicit integrator. We have chosen $\epsilon_t/k_t \sim 10^{-6}$, with ϵ_t antiparallel to $\mathbf{B}^{(0)}$. Thanks to the adaptivity of the integrator, we are able to resolve the resonant sheets, whose thickness scales with ϵ_t .

There are different ways to specify the nonmonochromatic magnetosheath fluctuations. Total pressure variations in the magnetosheath may be due to fluctuations of dynamic pressure (density or normal velocity variations), of thermal pressure (density variations), or of magnetic pressure (variations in field strength). In the simulations presented here, we impose density perturbations in the magnetosphere; the model then self-consistently computes the precise nature of the incident and reflected magnetosheath perturbations, which in general involve variations of all plasma and field parameters, not only of the density. The periodic density perturbation $s_{\text{msph}}(t)$ at the magnetospheric edge ($x = x_{\text{msph}}$, $y = z = 0$) has a Fourier expansion

$$s_{\text{msph}}(t) = \sum_{n=1}^{n_{\text{max}}} s_n e^{-i\omega_n t} + s_{-n} e^{+i\omega_n t}.$$

We limit n_{max} in order to keep all frequencies below the ion gyrofrequency. Note that s_{msph} is a real function of time, implying $s_n \equiv s_{-n}^*$ (the asterisk denotes the complex conjugate). Imposing $s_{\text{msph}}(t) = \rho^{(1)}(x_{\text{msph}}, t)$, or $s_n = \hat{\rho}_n(x_{\text{msph}})$, produces the desired linear combination of the spectral components that matches the driver. Note that, because C_1 and C_2 do not depend on the sign of ω_n , we also have $\hat{q}_n \equiv \hat{q}_{-n}^*$ for any perturbed quantity. Doing the inverse discrete Fourier transform, we necessarily obtain real perturbations $q^{(1)}(x, t)$. We choose the perturbation s_{msph} to have an arbitrarily small unit amplitude, as the solution is fixed only up to a scaling factor.

We have to stress here that the procedure outlined above does not always work: Waves that cannot propagate in the magnetosheath should not be present in the magnetospheric boundary condition, that is, we cannot arbitrarily choose the imposed waveform. We therefore modify the above procedure by setting $s_n = 0$ for those frequencies for which $\text{Re } K_x^2 < 0$ in the magnetosheath.

5. Solutions

We consider the low magnetic shear subsolar tangential discontinuity magnetopause, where the magnetic field $\mathbf{B}^{(0)}$ is along y . The base frequency is chosen to be $f_{\text{base}} = 5$ mHz. We use 100 frequencies in the Fourier description of the driver signal; the highest frequency does not exceed 500 mHz. We keep these frequencies fixed but consider two different cases depending on the tangential wave vector.

5.1. Intermittent Perturbations

In a first example we focus on the response of the magnetopause to individual density pulses, as an example of in-

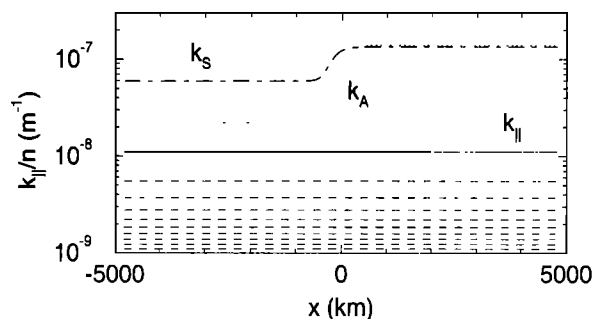


Figure 2. Wave vector diagram across the magnetopause for the first example (see text). The plot shows the Alfvén and slow-mode wave vectors $k_A(x)$ and $k_S(x)$ corresponding to the base frequency of the periodic incident signal, which vary by an order of magnitude across the magnetopause. The solid horizontal line corresponds to the wave vector k_{\parallel} of the incident wave; the dashed lines give the harmonics k_{\parallel}/n . Since there are no intersections between $k_A(x)$ or $k_S(x)$ and any of these harmonics, no resonant amplification can occur.

termittent perturbations. We use a periodic sequence (period is 200 s) of pairs of pulses of unit magnitude (in arbitrarily small units) with alternating sign. The wave vector is chosen to be $\mathbf{k}_t = [0.5, 0]k_{A, \text{msph}}$. The base frequency 5 mHz was chosen so as to ensure that all harmonic components remain in the MHD regime; on the other hand, the base period is sufficiently large (for the given wave vector) and the pulses are sufficiently far apart so that we can study the response of the magnetopause to an individual pulse without interference from other incident or reflected pulses. The tangential Alfvén wavelength at the magnetopause that corresponds to this frequency/wave vector combination is very large, of the order of the diameter of the magnetosphere. Each pulse lasts 10 s.

The base frequency wave and its harmonics are all propagating in both the magnetosheath and the magnetosphere ($\text{Re } K_x^2 > 0$). This is illustrated in Figure 2, which compares k_{\parallel}/n with the local Alfvén and slow-mode wave number profiles $k_A(x) = \omega_{\text{base}}/v_A$ and $k_S(x) = \omega_{\text{base}}/c_s$. In the cold plasma case the criterium $k_{\parallel}/n < k_A$ is a necessary and sufficient condition for propagation; in the warm case this condition still holds approximately if c_s is of the same order as v_A [De Keyser et al., 1999]. If the base frequency component is propagating, its harmonics are too.

Figure 3a shows the driving density perturbation s_{msph} imposed at the magnetospheric edge of the simulation domain. Figure 3b gives the power spectral density $P_{\text{msph}}(f)$ of this perturbation; most of the power is in the lowest frequencies. (The contribution of the higher frequencies increases for larger pulse width to period ratios.) Figure 3c plots the density perturbation $s_{\text{msh}}(t)$ at the magnetosheath edge of the domain, 5000 km upstream of the magnetopause, showing the alternating incident and reflected pulses. Note that the magnetosheath density fluctuation amplitude exceeds that in the magnetosphere by a factor 50. The power spectral density of the magnetosheath density fluctuations $P_{\text{msh}}(f)$ is given in Figure 3d.

The velocity and density perturbations $v_x^{(1)}(x, y = 0, z = 0, t)$ and $\rho^{(1)}(x, y = 0, z = 0, t)$ are given in Figure 4 as a function of distance x from the magnetopause and time t . The earthward traveling pulses of alternately earthward ($v_x^{(1)} < 0$) and sunward ($v_x^{(1)} > 0$) flow perturbations in the magnetosphere are caused by incident pulses in the magnetosheath (same $v_x^{(1)}$ sign), which also produce reflections (the echoes in Figure 3c). Figure 4 shows the successive effects of these alternating pulses. The vertical scales must be interpreted as being relative to the unit magnetospheric density perturbation amplitude. Near $t = 50$ s a positive pulse raises the density in the unperturbed magnetopause. At 100 s or -100 s a negative pulse brings the excess density at the magnetopause back to zero, near -50 s the next negative pulse forces a density depletion at the magnetopause, and, finally, near 0 s a positive pulse brings the magnetopause back to its unperturbed state. The net density change must be zero since the driver is periodic. The density perturbation is maximal in the magnetopause, where it has about 10 times the magnetosheath perturbation amplitude. The transmitted pulse density is only about 1/50th of the incident one.

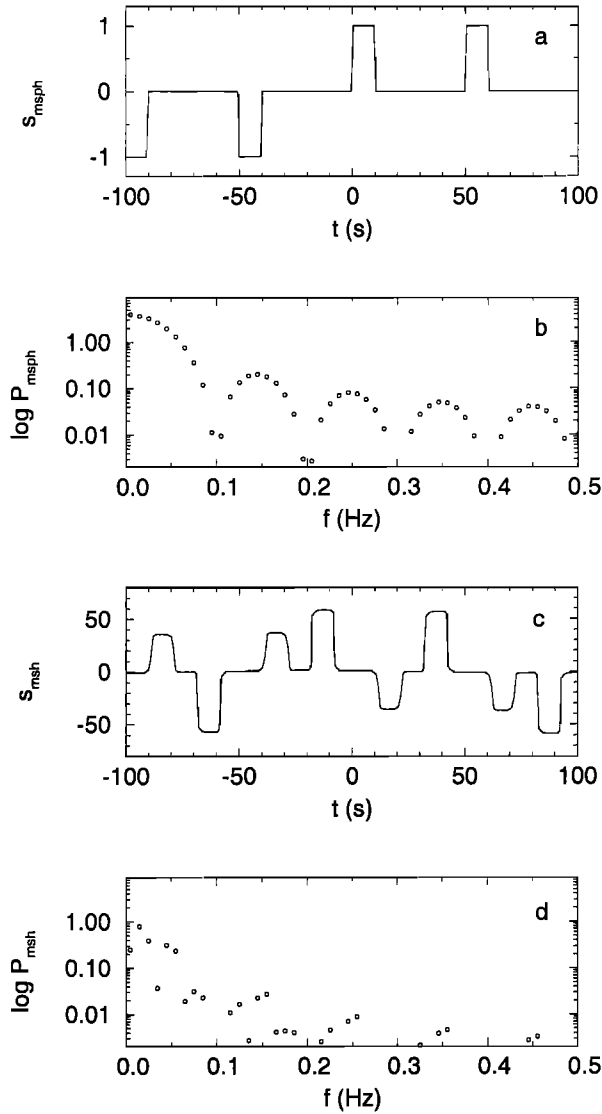


Figure 3. Driver perturbations for the first example (see text): (a) The specified density perturbation s_{msph} at the magnetospheric edge of the simulation domain, with an arbitrarily small unit amplitude, and (b) its power spectral density P_{msph} . (c) The corresponding perturbation s_{msh} at the magnetosheath edge of the domain, with an amplitude that is 50 times larger than that of the magnetospheric signal, showing the incident and reflected pulses, and (d) its power spectral density P_{msh} .

Let us focus on a single pulse, for instance, the incident enhanced density pulse arriving at the magnetopause near $t = 50$ s. Before the arrival of this pulse the magnetopause is in an essentially unperturbed state. When the pulse arrives, the density inside the magnetopause starts to increase. This increase continues progressively as long as the incident pulse lasts. Part of the pulse propagates across the magnetopause, but with a sharply reduced density. The propagating pulse is characterized by a faster group velocity: K_x is larger there because of the higher Alfvén and sound speeds, such that the phase velocities of the frequency components $v_{\text{ph}}(\omega) = \omega/K_x$ are all proportionally larger. A

reflected pulse is produced, which travels at the same speed as the incident one but in the opposite direction. This wave corresponds to a density reduction and an earthward flow perturbation, as though the strong density enhancement in the magnetopause transition requires some material from the magnetosheath to be pulled in.

Figure 5 illustrates the effect of the perturbation on the total density. We have superposed the perturbation on the equilibrium density, thereby choosing the perturbation amplitude large enough to be able to see its effect, but small enough so as to guarantee positivity of density and pressure everywhere. The effect of incident density enhancements is to bring plasma toward the magnetopause layer, thus shifting it more earthward, while incident density depletions allow the magnetopause to move outward again. Note that total pressure balance is satisfied up to first order at all times. The effect of a periodic pulse train is therefore an oscillating motion of the magnetopause over a distance of the order of the magnetopause thickness: The linear MHD response is controlled by the gradients of the unperturbed state; as soon as the perturbation is so large that it significantly alters the equilibrium (that is, when the location of the magnetopause significantly changes such that it no longer corresponds to the gradients of the unperturbed state) a nonlinear treatment is needed.

Considering time averages over a multiple of the pulse train period, we find that there is no net absorption of energy at the magnetopause. We define the integrated transmission, reflection, and absorption coefficients c_t , c_r , and c_a as the transmitted, reflected, and absorbed time-averaged flux relative to the incident time-averaged energy flux integrated over all frequencies; conservation of energy requires $c_t + c_r + c_a = 1$. In this example the time-averaged energy flux $\langle \phi_x \rangle$ is constant and negative (earthward), as shown in Figure 6a. The flux in the magnetosphere corresponds to the transmitted pulse, which carries $c_t = 53\%$ of the incident flux. The magnetosheath flux is the sum of the incident (negative) flux and the (positive) reflected flux (reflection coefficient $c_r = 47\%$). As there is no absorption ($c_a = 0\%$), the magnetosheath and magnetospheric fluxes are equal. Figure 6b plots the extreme values of the magnetic field perturbation; the amplitude of the ULF fluctuations clearly peaks at the magnetopause, while it is suppressed in the magnetosphere. It must be noted that there is a small and fluctuating normal magnetic field component B_x present in this perturbed tangential discontinuity magnetopause. This does not imply that the magnetopause becomes of the rotational discontinuity type but simply reflects the motion of the magnetic field lines associated with the wave; within the MHD frame, there can be no transfer of mass across the field lines at any time.

Figure 7 shows the spectral transmission, absorption and reflection coefficients $c_t(f)$, $c_a(f)$, and $c_r(f)$ in the 5 – 500 mHz range. For the given wave vector \mathbf{k}_t the transmission is enhanced as the frequency (and hence k_A and k_S) goes up; the reflection coefficient is correspondingly reduced. For none of the frequencies any absorption occurs.

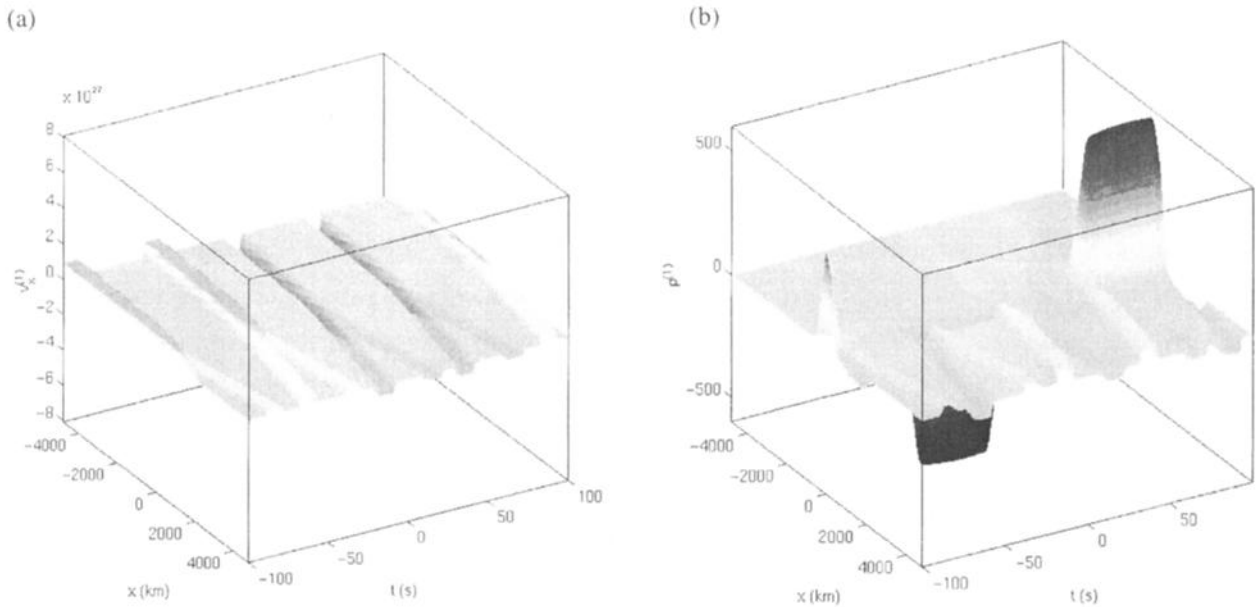


Figure 4. Perturbations for the first example. (a) Velocity perturbation along the Earth–Sun line. (b) Density perturbation, showing the strong magnetopause density enhancements or depletions produced by the incident positive or negative density pulses. The reflected and transmitted pulses are also visible, although the amplitude of the latter is very small. The scales are relative to the arbitrarily small unit magnetospheric density perturbation amplitude.

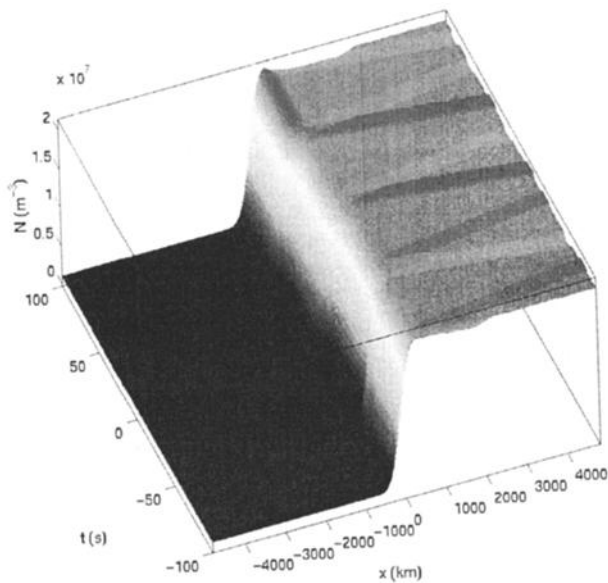


Figure 5. Spatiotemporal plot of the total number density N in the first example, when a fixed perturbation amplitude is chosen (small enough to remain within the linear regime, large enough so that it is visible in the figure). The incident positive and negative density perturbation pulses produce inward and outward magnetopause motion.

5.2. Response to a Broadband ULF Continuum

In the second example we study wave energy transport in the case of magnetosheath fluctuations with substantial

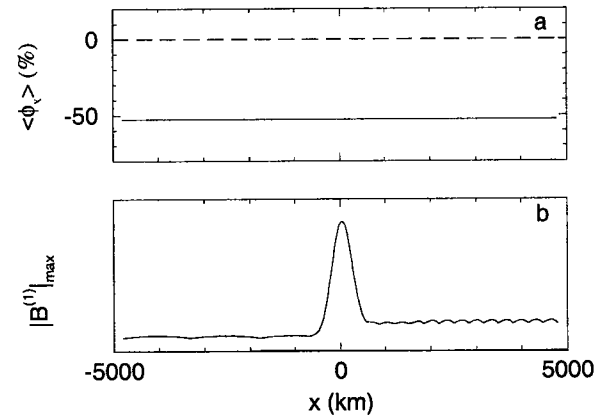


Figure 6. Resonant amplification characteristics for the first example: (a) The time averaged energy flux $\langle \phi_x(x) \rangle$ across the magnetopause remains constant and negative, indicating earthward energy flow and the absence of resonant absorption. (b) In spite of the absence of absorption, the maximum magnetic field perturbation $B_{\max}^{(1)}(x)$ (in arbitrary units) peaks at the magnetopause.

power in a broad low-frequency band; we use a spectrum that is qualitatively similar those reported by *Song et al.* [1994]. The tangential wave vector $k_t = [40, 40]k_{A, \text{msph}}$ is relatively large and corresponds to an Alfvén wavelength of 5000 km. The lowest frequency modes are nonpropagating in the magnetosheath and the magnetosphere, the intermediate frequency modes are propagating in the magnetosheath but nonpropagating in the magnetosphere, while the highest frequency modes are propagating everywhere (see Figure 8).

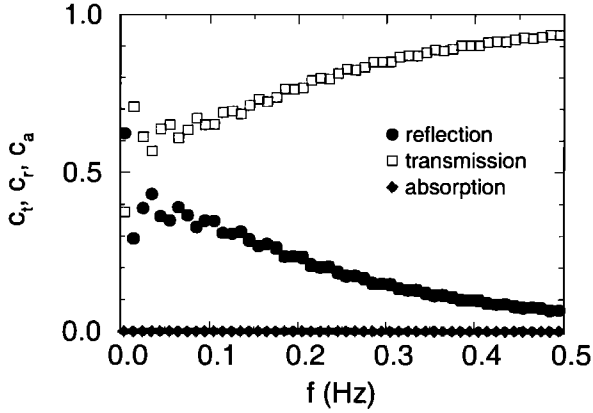


Figure 7. Spectral transmission, reflection, and absorption coefficients c_t , c_r , and c_a , in the first example.

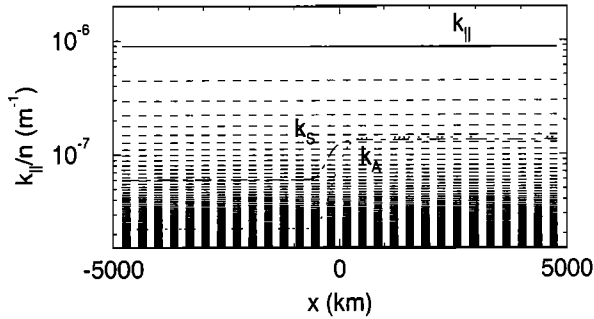


Figure 8. Wave vector diagram across the magnetopause for the second example (see text). The plot shows the Alfvén and slow-mode wave vectors $k_A(x)$ and $k_S(x)$ corresponding to the base frequency of the periodic incident signal, as they vary by an order of magnitude across the magnetopause. The solid horizontal line corresponds to the wave vector $k_{||}$ of the incident wave; the dashed lines give the harmonics $k_{||}/n$. The intersections between $k_A(x)$ or $k_S(x)$ and $k_{||}/n$ correspond to mode conversion sites where resonant amplification occurs.

For the base frequency and the modes up to $n = 6$, $k_{||}/n$ lies above the k_A and k_S profiles. There is a broad band of modes for which $k_{||}/n$ matches k_A and/or k_S at some point inside the magnetopause transition, giving rise to Alfvén or slow-mode resonances. For the highest frequency part of the spectrum, $k_{||}/n$ remains below the k_A and k_S profiles.

Figure 9a shows the driver s_{msph} in the magnetosphere (solid line), which is obtained by filtering away the lowest frequencies from the originally proposed pulse train (dashed line): Since these modes are nonpropagating in the magnetosheath, the periodic square pulse signal cannot exist in the magnetosphere. Figure 9b gives the power spectral density $P_{\text{msph}}(f)$ of this perturbation. Figure 9c shows the corresponding perturbation s_{msh} in the magnetosheath. The frequency components that do not propagate in the magnetosphere dominate s_{msh} (Figure 9d); otherwise, they should have essentially vanished by the time they reach the magnetospheric edge of the simulation domain, in which case they would be absent from the magnetospheric signal s_{msph} .

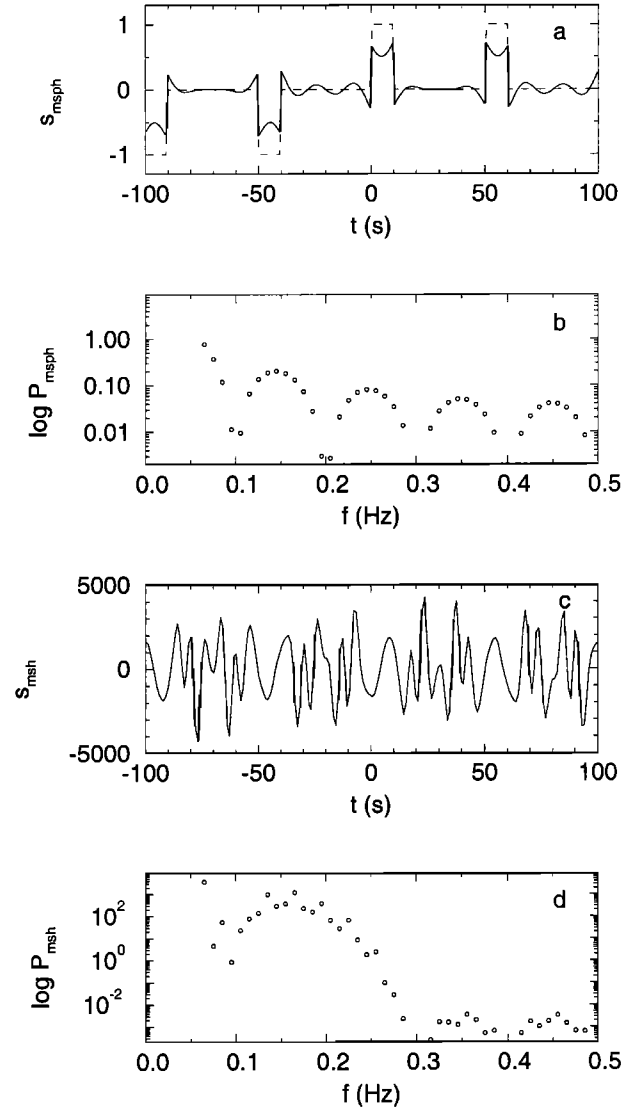


Figure 9. Driver perturbations for the second example (see text): (a) The specified perturbation s_{msph} at the magnetospheric edge of the simulation domain (solid line) and the pulse train it is obtained from by filtering away the low-frequency modes that do not propagate in the magnetosheath (dashed line), and (b) its power spectral density P_{msph} . (c) The corresponding incident perturbation s_{msh} (the scale is relative to the unit magnetospheric density perturbation amplitude), and (d) its power spectral density P_{msh} , illustrating the dominant presence of modes that do not propagate in the magnetosphere.

Note the substantial fluctuation power in the 50–300 mHz band.

Figure 10 plots the density fluctuation $\rho^{(1)}(x, y = 0, z = 0, t)$. Interference occurs between incident and reflected waves in the magnetosheath. The magnitude of the density perturbations in the magnetosphere is strongly reduced, by a factor 5000. The peaks situated at $x = -600$ km correspond to a site of resonance with strong effect on the density.

The resonant absorption is most easily identified in plots of the energy flux profile and of the maximum magnetic field perturbation (Figures 11a and 11b). While the energy flux

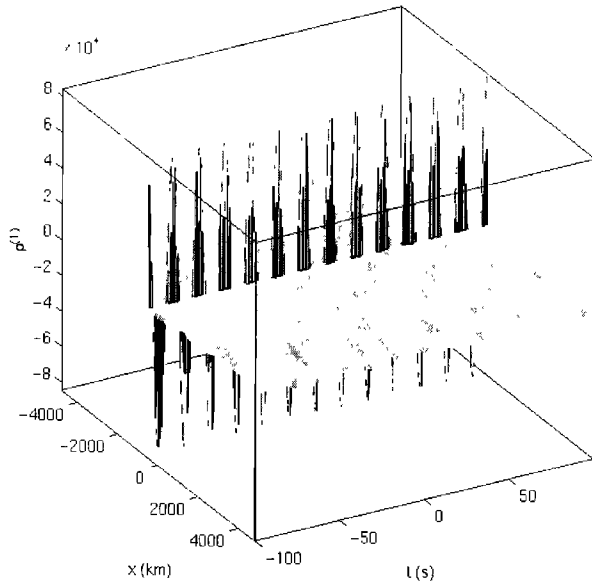


Figure 10. Density perturbation for the second example. The density peaks witness the resonant behavior inside the magnetopause transition. The density scale is relative to the unit magnetospheric density perturbation amplitude.

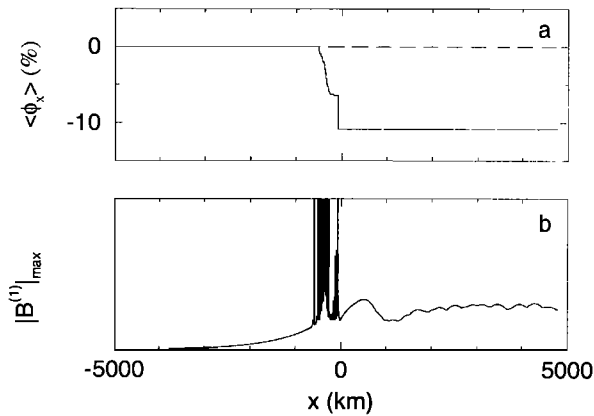


Figure 11. Resonant amplification characteristics for the second example: (a) The time averaged energy flux $\langle \phi_x(x) \rangle$ changes across the magnetopause due to resonant absorption; the staircase-like jumps arise from the use of a discrete rather than a continuous spectrum. (b) Sharp peaks in the maximum magnetic field perturbation $B_{\max}^{(1)}(x)$ (in arbitrary units) indicate that resonant behavior occurs throughout large parts of the magnetopause.

makes a discrete jump at each individual resonance, the discrete spectrum used here is so close to a continuous one that the energy flux profile resembles a smooth continuous curve rather than a staircase line, at least in the earthward part of the magnetopause layer. The magnetic field perturbation has a very irregular appearance, with a succession of closely spaced peaks that are, in principle, infinitely narrow and high (as $\text{Im } k_t \rightarrow 0$) and that correspond to mode resonances throughout the magnetopause transition. A quantitative estimate of the resonant amplification factor is impos-

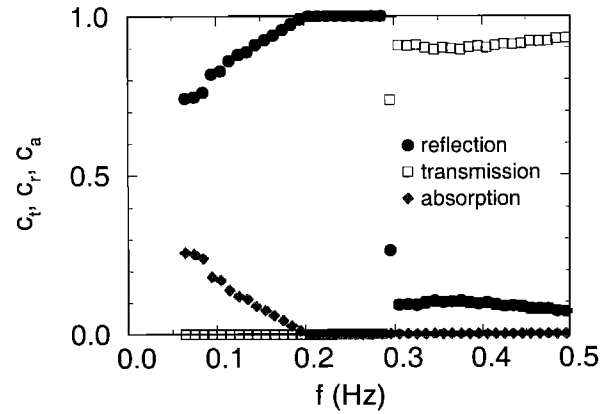


Figure 12. Spectral transmission, reflection, and absorption coefficients c_t , c_r , and c_a , for the second example. Note the abrupt changes in these coefficients at 300 mHz, where the magnetosphere becomes transparent for the incident waves.

sible within the ideal MHD framework (the amplification is infinite). The mode conversion process drives the excitation of surface waves on the magnetopause with the prescribed 5000 km tangential wavelength. The fluctuating B_x component witnesses the bending of the magnetic field lines due to this surface wave, while there is no mass transport across the field lines.

Figure 12 shows the spectral transmission, absorption, and reflection coefficients. Frequencies below 50 mHz are not present in the incident signal. Below 300 mHz the spectral transmission coefficient is zero as such waves do not propagate in the magnetosphere. These waves are characterized by partial absorption and partial reflection; the spectral absorption is stronger for lower frequencies, while reflection off the magnetopause occurs more easily for the highest of these frequencies. Above 300 mHz the magnetosphere becomes transparent, such that about 90% of the incident flux is transmitted. In the particular example shown here, the integrated transmission coefficient is about 0%, the integrated absorption amounts to 11%, while 89% is reflected. The small integrated transmission in spite of the high spectral transmission above 300 mHz is due to the negligible contribution of the highest frequency components in the incident perturbation s_{msh} .

6. Discussion

This paper evaluates a scenario for the transport of electromagnetic energy present in magnetosheath ULF fluctuations to the magnetopause. The calculations have been carried out in the framework of linear ideal MHD. The particular contribution of this paper is twofold: (1) We have extended earlier work concerning resonant amplification of monochromatic MHD waves at the magnetopause [Belmont *et al.*, 1995; De Keyser *et al.*, 1999] to the case of incident waves with a broad frequency content. (2) We have computed the magnetopause response to both intermittent and continuous small-amplitude broadband ULF hydromagnetic waves.

In a first example we have considered intermittent small-amplitude MHD waves in the form of individual density pulses arriving at a stationary magnetopause. Our simulations illustrate that an obvious effect of such pulses is a small-scale motion of the magnetopause, in addition to fluctuations in other plasma and field parameters, including small density enhancements near the magnetopause. The linear MHD limitation manifests itself in the fact that the maximum distance of motion is of the order of the magnetopause thickness itself. Both small- and large-amplitude motion of the magnetopause (over distances exceeding the magnetopause thickness) are well known from observations [Song *et al.*, 1988].

In a second example we have studied the effect of broadband fluctuations. The simulations offer a fairly realistic view of the magnetopause response to such a broadband signal. Perraut *et al.* [1979], Anderson *et al.* [1982], and Song *et al.* [1994] confirm the presence of such broadband compressional waves in the inner magnetosheath; other wave modes appear to dominate in the outer magnetosheath. The computations illustrate that ideal MHD resonant behavior in general does not lead to an individual singular layer inside the magnetopause but that the resonant process is spread out more evenly throughout the transition, leading to a relatively wide region characterized by magnetic field and density irregularities. Such irregularities might be important for diffusive transport of mass across the layer. While no such transport can be present in an ideal MHD description, the inclusion of inertial effects would lead to substantial mass transport [Winske and Omidi, 1995]. Treumann *et al.* [1995] even suggest that the ULF waves can provide sufficient diffusion to form the low-latitude boundary layer. As such mass transport would alter the ion and electron density profiles in the magnetopause current layer, it would affect the time evolution of the charge separation electric field inside the magnetopause that is constantly discharged in the ionosphere [Willis, 1970].

We have deliberately not studied the case of a zero-order motion of the magnetopause in order to avoid a number of complications. Because of the discharge of the electrostatic field at the magnetopause through the ionosphere, a one-dimensional tangential discontinuity magnetopause might appear impossible altogether. This discharge, however, can easily be balanced by the continuous replenishment of the charge carriers responsible for the charge imbalance that produces the electrostatic field. The resulting dynamic equilibrium therefore remains essentially a one-dimensional tangential discontinuity equilibrium. Consider now a slow zero-order motion, that is, a magnetopause velocity v_{MP} less than the ratio of the magnetopause thickness divided by the characteristic time, or thickness times frequency: $v_{MP} < 1.5 \text{ km s}^{-1}$ in the first example for the 5 mHz base frequency, and $v_{MP} < 15\text{-}90 \text{ km s}^{-1}$ in the second application for the 50-300 mHz band in which most of the signal power is concentrated. In this case the stationary magnetopause analysis holds essentially unmodified. Otherwise, for a faster zero-order motion, the coupling to the ionosphere

will introduce a spatial gradient in the structure of the magnetopause along the magnetopause surface. Only for sufficiently small wavelengths the one-dimensional approximation can be justified. The present analysis can then be applied in a frame comoving with the magnetopause, if one accounts for the Doppler shift associated with the frame transformation. Note also that the earthward state should change as the magnetopause moves. And then there is the question to what extent the magnetopause is accelerating or decelerating. As the magnetopause is observed to have speeds that are of the order of the slow-/high-speed motion threshold, it can be concluded that the overall response of the magnetopause will not be affected by zero-order motion, although the details of the interaction are expected to depend on it.

The linear ideal MHD approximation has several limitations. It can only be used to describe waves with frequencies below the proton gyrofrequency, while observations show that the fluctuation spectra extend beyond the proton gyrofrequency. Ideal MHD does not allow to quantitatively estimate the resonant amplification factor. The linear description breaks down in resonant layers as the perturbation amplitude becomes infinite there. A nonlinear approach [Song *et al.*, 1998] and the inclusion of kinetic effects are inevitable for a more realistic description [Lacombe *et al.*, 1995; Johnson and Cheng, 1997]. Another limitation of the present model is the absence of any coupling with the ionosphere. The model therefore gives only a qualitative description. Nevertheless, our simulations of mode conversion reflect some of the observed characteristics of the magnetopause: rapid small-scale magnetopause motion, the enhanced ULF fluctuation amplitudes throughout the magnetopause layer and the suppression of such fluctuations in the magnetosphere. We also note the presence of a small fluctuating normal magnetic field component in magnetopause configurations that otherwise display tangential discontinuity characteristics. Such normal magnetic field variations, which are also frequently seen in a minimum variance analysis of magnetopause observations, are interpreted in this context as the signature of the small-scale nonplanarity of the magnetopause surface due to surface waves.

We have used in this paper a superposition of waves of the form $e^{i(\mathbf{k}_t \cdot \mathbf{r} - \omega t)}$ by keeping \mathbf{k}_t fixed and summing over different frequencies, which has allowed us to model the magnetopause response to temporally localized plane wave pulses. It is interesting to note the formal similarity of this procedure with the superposition of waves produced by keeping ω fixed and summing over different wave vectors. This allows one to study the magnetopause response to spatially localized pulses. One can also consider Fourier decompositions in both space and time, so as to produce spatially and temporally localized pulses, that is, incident blobs with slightly enhanced density. Incoherent turbulence could be studied in the same manner. Similar to the results presented here, the linear MHD description would apply to density fluctuations that are so small that they would perturb the magnetopause position only slightly.

A1. Appendix A: Linearized MHD Equations

This appendix briefly describes the linearization of the static ideal MHD equations [see Walker, 1981; De Keyser et al., 1999]. Let x be the normal to the plasma sheet, ρ be the mass density, \mathbf{v} be the bulk velocity, and \mathbf{B} and \mathbf{E} be the magnetic and electric fields. The thermal pressure is $p = k_B \rho T / m$, where k_B is Boltzmann's constant, m the (ion + electron) mass, and T the (ion + electron) temperature. The specific energy is $\mathcal{E} = \rho v^2 / 2 + B^2 / 2\mu_0 + p / (\gamma - 1)$, where $\gamma = \frac{5}{3}$ is the ratio of specific heats. The ideal MHD equations are

$$\frac{\partial \rho}{\partial t} + \nabla \cdot (\rho \mathbf{v}) = 0, \quad (\text{A1})$$

$$\frac{\partial \rho \mathbf{v}}{\partial t} + \nabla \cdot [\rho \mathbf{v} \mathbf{v} + (p + \frac{B^2}{2\mu_0}) \mathbf{I} - \frac{1}{\mu_0} \mathbf{B} \mathbf{B}] = 0, \quad (\text{A2})$$

$$\frac{\partial \mathcal{E}}{\partial t} + \nabla \cdot [(\frac{\rho v^2}{2} + \frac{\gamma p}{\gamma - 1}) \mathbf{v} + \frac{1}{\mu_0} \mathbf{E} \times \mathbf{B}] = 0. \quad (\text{A3})$$

Ideal MHD includes only the convection electric field, and Maxwell's equations become

$$\mathbf{E} + \mathbf{v} \times \mathbf{B} = \mathbf{0}, \quad (\text{A4})$$

$$\frac{\partial \mathbf{B}}{\partial t} + \nabla \times \mathbf{E} = \mathbf{0}, \quad (\text{A5})$$

$$\nabla \cdot \mathbf{B} = 0. \quad (\text{A6})$$

Let $\xi(\mathbf{r}, t)$ denote the current position of a plasma element that was at position \mathbf{r} at a reference time t_0 ; then

$$\mathbf{v} = \frac{d\xi}{dt} = \frac{\partial \xi}{\partial t} + (\mathbf{v} \cdot \nabla) \xi. \quad (\text{A7})$$

We also define the total pressure by

$$\tau = p + \frac{B^2}{2\mu_0}. \quad (\text{A8})$$

We write all quantities in the form $q(\mathbf{r}, t) = q^{(0)}(x) + q^{(1)}(\mathbf{r}, t) + q^{(2)}(\mathbf{r}, t) + \dots$ where $q^{(0)}$ is the equilibrium state, and $q^{(1)}$ and $q^{(2)}$ are the first- and second-order perturbations. We consider monochromatic waves with frequency $\omega = \pm 2\pi f$ and tangential wave vector $\mathbf{k}_t = [0, k_y, k_z]$ of the form $q^{(1)} = \hat{q}(x) e^{i(\mathbf{k}_t \cdot \mathbf{r} - \omega t)}$. The second-order perturbations are waves with frequencies $\omega \pm \omega$: a DC and a double frequency component. We denote the average of $q^{(2)}$ over y , z , and t (that is, the DC component) by $\langle q^{(2)}(x) \rangle$. The spatial derivatives are given by the operator $\nabla \equiv [d/dx, 0, 0]$ for equilibrium quantities, and by $\hat{\nabla} \equiv [d/dx, ik_y, ik_z]$ for first-order perturbations. The time derivatives are $d/dt \equiv 0$ for zero-order quantities, and $d/dt \equiv (-i\omega)$ for first-order quantities.

Accounting for the static tangential discontinuity equilibrium that is used here, with $B_x^{(0)} \equiv 0$ and $\mathbf{v}^{(0)} \equiv \mathbf{0}$, the zero-order equations reduce to $d\tau^{(0)}/dx = 0$, that is, the pressure balance condition. Defining $\kappa_0 = k_t B^{(0)}$, the first-order equations are

$$\begin{aligned} -i\omega \hat{\rho} + (\hat{\nabla} \cdot \hat{\mathbf{v}} + \hat{\mathbf{v}} \cdot \nabla) \rho^{(0)} &= 0, \\ -i\omega \rho^{(0)} \hat{\mathbf{v}} + \hat{\nabla} \hat{\tau} - \frac{1}{\mu_0} [(\hat{\mathbf{B}} \cdot \nabla) \mathbf{B}^{(0)} + i\kappa_0 \hat{\mathbf{B}}] &= 0, \\ -i\omega (\hat{p} - c_s^2 \hat{\rho}) + \hat{\mathbf{v}} \cdot \nabla p^{(0)} - c_s^2 \hat{\mathbf{v}} \cdot \nabla \rho^{(0)} &= 0, \\ \hat{\mathbf{E}} + \hat{\mathbf{v}} \times \mathbf{B}^{(0)} &= 0, \\ -i\omega \hat{\mathbf{B}} - i\kappa_0 \hat{\mathbf{v}} + (\hat{\nabla} \cdot \hat{\mathbf{v}} + \hat{\mathbf{v}} \cdot \nabla) \mathbf{B}^{(0)} &= 0, \\ \hat{\nabla} \cdot \hat{\mathbf{B}} &= 0, \\ i\omega \hat{\xi} + \hat{\mathbf{v}} &= 0, \\ -\hat{\tau} + \hat{p} + \frac{1}{\mu_0} \mathbf{B}^{(0)} \cdot \hat{\mathbf{B}} &= 0, \end{aligned}$$

where $c_s^2 = \gamma p^{(0)} / \rho^{(0)}$ defines the local sound speed. We solve for $\hat{\xi}_x$ and $\hat{\tau}$:

$$\frac{d}{dx} \hat{\tau} = C_1 \hat{\xi}_x = \rho^{(0)} \Omega_{kA}^2 \hat{\xi}_x,$$

$$\frac{d}{dx} \hat{\xi}_x = C_2 \hat{\tau} = -\left(\frac{\omega^2}{v_A^2 + c_s^2 \Omega_{kA}^2 / \omega^2} - k_t^2 \right) \frac{\hat{\tau}}{\rho^{(0)} \Omega_{kA}^2},$$

where $\Omega_{kA}^2 = \omega^2 - \omega_{kA}^2$ and $\omega_{kA} = \mathbf{k}_t \cdot \mathbf{v}_A$, with the Alfvén velocity $\mathbf{v}_A = \mathbf{B}^{(0)} / \sqrt{\mu_0 \rho^{(0)}}$. The other perturbations are

$$\hat{\rho} = -\frac{d\rho^{(0)}}{dx} \hat{\xi}_x + \frac{\hat{\tau}}{v_A^2 + c_s^2 \Omega_{kA}^2 / \omega^2},$$

$$\hat{p} = -\frac{dp^{(0)}}{dx} \hat{\xi}_x + \frac{c_s^2 \hat{\tau}}{v_A^2 + c_s^2 \Omega_{kA}^2 / \omega^2},$$

$$\hat{v}_x = -i\omega \hat{\xi}_x,$$

$$\hat{v}_y = \frac{\omega}{\rho^{(0)} \Omega_{kA}^2} \left(k_y - \frac{\omega_{kA} v_{Ay}}{v_A^2 + c_s^2 \Omega_{kA}^2 / \omega^2} \right) \hat{\tau},$$

$$\hat{v}_z = \frac{\omega}{\rho^{(0)} \Omega_{kA}^2} \left(k_z - \frac{\omega_{kA} v_{Az}}{v_A^2 + c_s^2 \Omega_{kA}^2 / \omega^2} \right) \hat{\tau},$$

$$\hat{B}_x = i\kappa_0 \hat{\xi}_x,$$

$$\hat{B}_y = -\frac{dB_y^{(0)}}{dx} \hat{\xi}_x + \left(-\kappa_0 k_y + \frac{\omega^2 B_y^{(0)}}{v_A^2 + c_s^2 \Omega_{kA}^2 / \omega^2} \right) \frac{\hat{\tau}}{\rho^{(0)} \Omega_{kA}^2},$$

$$\hat{B}_z = -\frac{dB_z^{(0)}}{dx} \hat{\xi}_x + \left(-\kappa_0 k_z + \frac{\omega^2 B_z^{(0)}}{v_A^2 + c_s^2 \Omega_{kA}^2 / \omega^2} \right) \frac{\hat{\tau}}{\rho^{(0)} \Omega_{kA}^2}.$$

The mass flux vector is $\psi = \rho \mathbf{v}$. The time-averaged mass flux across the magnetopause is

$$\langle \psi_x \rangle = \langle \psi_x^{(2)} \rangle = \frac{\omega}{2} \frac{d\rho^{(0)}}{dx} \text{Im} \{ \hat{\xi} \hat{\xi}^* \} = 0,$$

where the asterisk denotes complex conjugation. The energy flux vector is

$$\phi = \left(\frac{\rho v^2}{2} + \frac{\gamma p}{\gamma - 1} \right) \mathbf{v} + \frac{1}{\mu_0} \mathbf{E} \times \mathbf{B}.$$

The time-averaged normal energy flux is

$$\langle \phi_x \rangle = \langle \phi_x^{(2)} \rangle = \frac{\omega}{2} \text{Im} \{ \hat{\xi}_x \hat{\tau}^* \}.$$

The energy flux change over an interval $[a, b]$ is given by

$$\Delta\langle\phi_x\rangle = \int_a^b \left(\frac{d}{dx}\langle\phi_x\rangle\right) dx = \frac{\omega}{2} \int_a^b \operatorname{Im} \{C_1^* \hat{\xi}_x \hat{\xi}_x^* + C_2 \hat{\tau} \hat{\tau}^*\} dx.$$

Using Cauchy's theorem at the singular points, we find

$$\Delta\langle\phi_x\rangle = \frac{\omega\pi}{2} \sum_{x_\alpha} \pm \lim_{x \rightarrow x_\alpha} (x - x_\alpha) [C_1^* \hat{\xi}_x \hat{\xi}_x^* + C_2 \hat{\tau} \hat{\tau}^*],$$

where the sum extends over all singular points x_α in the interval. In the absence of singularities, $\langle\phi_x\rangle$ remains constant. Otherwise, the energy flux changes discontinuously at each x_α . The signs of the jumps depend on how the integration path in the complex plane is chosen when applying the Cauchy theorem.

Acknowledgments. The author wants to thank Michel Roth for valuable discussions. This work was supported by a PRODEX contract with ESA in the framework of the Cluster II project. The support of the Belgian Federal Office for Scientific, Technical and Cultural Affairs is acknowledged.

Michel Blanc thanks Paul Song and Gérard Belmont for their assistance in evaluating this paper.

References

- Anderson, R. R., C. C. Harvey, M. M. Hoppe, B. T. Tsurutani, T. E. Eastman, and J. Etcheto, Plasma waves near the magnetopause, *J. Geophys. Res.*, **87**, 2087–2107, 1982.
- Belmont, G., F. Reberac, and L. Rezeau, Resonant amplification of magnetosheath MHD fluctuations at the magnetopause, *Geophys. Res. Lett.*, **22**, 295–298, 1995.
- Berchem, J., and C. T. Russell, The thickness of the magnetopause current layer: ISEE 1 and 2 observations, *J. Geophys. Res.*, **87**, 2108–2114, 1982.
- De Keyser, J., M. Roth, F. Reberac, L. Rezeau, and G. Belmont, Resonant amplification of MHD waves in realistic subsolar magnetopause configurations, *J. Geophys. Res.*, **104**, 2399–2409, 1999.
- Engebretson, M. J., N. Lin, W. Baumjohann, H. Lühr, B. J. Anderson, L. J. Zanetti, T. A. Potemra, R. L. McPherron, and M. G. Kivelson, A comparison of ULF fluctuations in the solar wind, magnetosheath, and dayside magnetosphere, 1, Magnetosheath morphology, *J. Geophys. Res.*, **96**, 3441–3454, 1991.
- Hollweg, J. V., A simple mechanical model for resonance absorption: The Alfvén resonance, *J. Geophys. Res.*, **102**, 24,127–24,137, 1997.
- Johnson, J. R., and C. Z. Cheng, Kinetic Alfvén waves and plasma transport at the magnetopause, *Geophys. Res. Lett.*, **24**, 1423–1426, 1997.
- LaBelle, J., and R. A. Treumann, Plasma waves at the dayside magnetopause, *Space Sci. Rev.*, **47**, 175–202, 1988.
- Lacombe, C., G. Belmont, D. Hubert, C. C. Harvey, A. Mangeney, C. T. Russell, J. T. Gosling, and S. A. Fuselier, Density and magnetic field fluctuations observed by ISEE 1-2 in the quiet magnetosheath, *Ann. Geophys.*, **13**, 343–357, 1995.
- Lee, L. C., and J. R. Kan, A unified kinetic model of the tangential magnetopause structure, *J. Geophys. Res.*, **84**, 6417–6426, 1979.
- Paschmann, G., B. U. Ö. Sonnerup, I. Papamastorakis, N. Scokopke, G. Haerendel, S. J. Bame, J. R. Asbridge, J. T. Gosling, C. T. Russell, and R. C. Elphic, Plasma acceleration at the Earth's magnetopause: Evidence for reconnection, *Nature*, **282**, 243–246, 1979.
- Perraut, S., R. Gendrin, P. Robert, and A. Roux, Magnetic pulsations observed on board GEOS-2 in the ULF range during multiple magnetopause crossings, in *Proceedings of the Magnetospheric Boundary Layers Conference*, Eur. Space Agency Spec. Publ. ESA SP 148, 113–122, 1979.
- Poedts, S., M. Goossens, and W. Kerner, Numerical simulation of coronal heating by resonant absorption of Alfvén waves, *Sol. Phys.*, **123**, 83–115, 1989.
- Rezeau, L., A. Morane, S. Perraut, A. Roux, and R. Schmidt, Characterization of Alfvénic fluctuations in the magnetopause boundary layer, *J. Geophys. Res.*, **94**, 101–110, 1989.
- Rezeau, L., A. Roux, and C. T. Russell, Characterization of small-scale structures at the magnetopause from ISEE measurements, *J. Geophys. Res.*, **98**, 179–186, 1993.
- Song, P., R. C. Elphic, and C. T. Russell, ISEE 1 and 2 observations of the oscillating magnetopause, *Geophys. Res. Lett.*, **15**, 744–747, 1988.
- Song, P., C. T. Russell, and C. Y. Huang, Wave properties near the subsolar magnetopause: Pc 1 waves in the sheath transition layer, *J. Geophys. Res.*, **98**, 5907–5923, 1993.
- Song, P., C. T. Russell, and S. P. Gary, Identification of low-frequency fluctuations in the terrestrial magnetosheath, *J. Geophys. Res.*, **99**, 6011–6025, 1994.
- Song, P., C. T. Russell, and L. Chen, On large-amplitude MHD waves in high-beta plasma, *J. Geophys. Res.*, **103**, 29,569–29,580, 1998.
- Sonnerup, B. U. Ö., and L. J. Cahill Jr., Explorer 12 observations of the magnetopause current layer, *J. Geophys. Res.*, **73**, 1757–1770, 1968.
- Southwood, D. J., Some features of field line resonances in the magnetosphere, *Planet. Space Sci.*, **22**, 483–491, 1974.
- Treumann, R. A., J. LaBelle, and T. M. Bauer, Diffusion processes: An observational perspective, in *Physics of the Magnetopause*, *Geophys. Mon. Ser.*, vol. 90, edited by P. Song, B. Sonnerup, and M. F. Thomsen, pp. 331–341, AGU, Washington, D.C., 1995.
- Walker, A. D. M., The Kelvin-Helmholtz instability in the low-latitude boundary layer, *Planet. Space Sci.*, **29**, 1119–1133, 1981.
- Willis, D. M., The electrostatic field at the magnetopause, *Planet. Space Sci.*, **18**, 749–769, 1970.
- Winske, D., and N. Omidi, Diffusion at the magnetopause: Hybrid simulations, *J. Geophys. Res.*, **100**, 11,923–11,933, 1995.
- Zhu, X., and M. G. Kivelson, Global mode ULF pulsations in a magnetosphere with a nonmonotonic Alfvén velocity profile, *J. Geophys. Res.*, **94**, 1479–1485, 1989.

J. De Keyser, Belgian Institute for Space Aeronomy, Ringlaan 3, B-1180 Brussels, Belgium. (Johan.DeKeyser@bira-iasb.oma.be)

(Received December 27, 1999; revised May 18, 2000; accepted May 24, 2000.)